Steady-state gain and saturation flux measurements in a high efficiency, electron-beam-pumped, Ar-Xe laser

Thomas T. Perkins[a)]
Science Research Laboratory, Inc., 15 Ward Street, Somerville, Massachusetts 02143

Flat-top, Ar-Xe laser pulses at 1.73 μm have been achieved by pumping the laser medium with a constant-current electron beam for pulse durations of up to 2.5 ms. The 220 keV electron beam pumped an active volume of $50 \times 8 \times 6$ cm^3 at power loadings of 6–100 W/cm^3. Small signal gain, saturation flux, and nonsaturable absorption were determined as a function of Xe concentration, total gas pressure, and pump power density by a Rigrod analysis. In the experimental regime investigated, the small signal gain increased as the total laser pressure decreased and as the partial pressure of Xe decreased. The Xe concentration was varied from 0.5% to 2.0% and the total pressure was varied from 250 to 860 Torr. The results are consistent with Xe quenching of the upper laser level being the dominant deexcitation process and with the collisional broadening dominating the linewidth. The peak intrinsic efficiency observed was 2.2%.

I. INTRODUCTION

The high pressure argon-xenon laser has several attractive features including high efficiency, inert gas mixture, and scalability to large apertures. Efficiencies of 2%–6% have been demonstrated using electron-beam pumping,[1–7] electron-beam-controlled discharges,[1,8,9] x-ray preionized discharges,[10] and fission-fragment pumping.[11–13] Efficient operation has been observed on the 1.73, 2.03, and 2.65 μm transitions. The most efficient operation is at 1.73 μm, corresponding to the $5d[3/2]_1 \rightarrow 6p[5/2]_2$ atomic transition in Xe.

Ar-Xe lasers have significant gain (0.5%/cm–1%/cm) at pump power densities as low as 10 W/cm^3. Since the active medium has no measurable nonsaturable loss, the stored optical power can be efficiently extracted. This makes Ar-Xe lasers a potentially attractive choice for long pulse or cw operation by electron-beam pumping. In this investigation, the steady-state behavior of an Ar-Xe laser was studied using low-power, long-pulse, electron-beam pumping. Fission-fragment pumping also uses long-pulse, low-power, operation and the excited state kinetics of fission-fragment excitation are similar to electron-beam pumping.[14] Thus, results from this experiment can yield insight into fission-fragment pumping and, more generally, the complicated electron kinetics of an Ar-Xe laser. To achieve long-pulse operation, a thermionic cathode provided a constant-current electron beam with durations up to 2.5 ms. The resulting optical pulses were flat-top verifying that steady-state laser operation has been achieved. Millisecond-duration, electron-beam-pumped Ar-Xe lasers have been previously demonstrated in both transverse[7] and coaxial[4] geometries. In the coaxial electron-beam pumping described by Patterson *et al.*,[4] the laser pulse self-terminated at a specific energy loading of 0.178 J/cm^3 atm, which may represent a specific energy loading limit for this laser.[15] In this research, the steady-state values of the small signal gain (g_0), the saturation flux (Φ_{sat}), and the nonsaturable absorption (α_{ns}) were determined for the 1.73 μm transition. These important laser parameters have been previously characterized using temporally varying pulses at low pump power densities of 5–30 W/cm^3 by fission fragment excitation[11,13,16] and moderate pump power densities of 2–16 kW/cm^3 by electron-beam pumping.[2] We report steady-state values of these parameters determined by a Rigrod[17] analysis from flat-top, 100 μs long optical pulses for various Xe concentrations, total gas mixture pressures, and pump power densities. For one such analysis of a 0.5% Xe mixture at a total gas pressure of 250 Torr pumped at 20 W/cm^3, g_0, Φ_{sat}, and α_{ns} were determined to be 1.03±0.04%/cm, 40.9±1.6 W/cm^2, and $2\pm2\times10^{-5}$%/cm, respectively, where α_{ns} is zero within experimental error. In general, g_0 decreased with both increasing pressure and with increasing Xe partial pressure. But, importantly, the intrinsic efficiency remained constant at approximately 2.2%.

A. The kinetics of electron beam pumping

When a typical Ar-Xe laser gas mixture is pumped by high-energy electrons (e_h), approximately 60% of the beam power deposited goes into the formation of electron-ion pairs via the following reaction:

$$e_h + \text{Ar} \rightarrow \text{Ar}^+ + e + e_h. \tag{1}$$

The atomic argon ions Ar$^+$ rapidly form molecular ions Ar$_2^+$ by three body recombination:

$$\text{Ar}^+ + 2\text{Ar} \rightarrow \text{Ar}_2^+ + \text{Ar}. \tag{2}$$

The molecular ions in turn create xenon atomic ions by charge transfer:

$$\text{Ar}_2^+ + \text{Xe} \rightarrow \text{Xe}^+ + 2\text{Ar}. \tag{3}$$

The Xe ions then rapidly form heteronuclear ions and xenon molecular ions via the following reactions:

[a)]Present address: Dept. of Physics, Stanford University, Stanford, CA 94305.
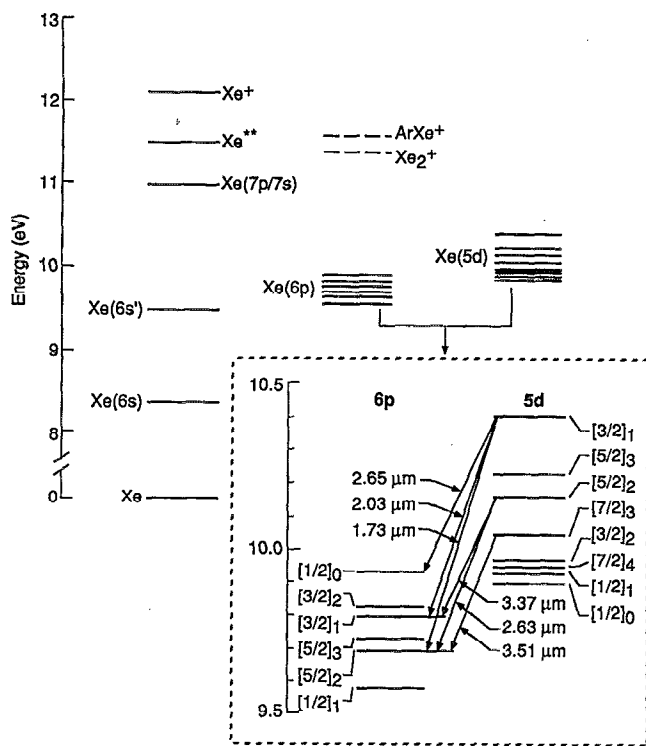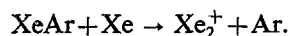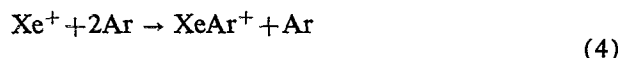
FIG. 1. Energy level diagram for an Ar-Xe laser showing the 5d and 6p manifolds of atomic xenon and the dominant laser transitions (from Ref. 14).

$$Xe^+ + 2Ar \rightarrow XeAr^+ + Ar$$
$$XeAr + Xe \rightarrow Xe_2^+ + Ar. \qquad (4)$$

These molecular ions then dissociatively recombine with electrons to form Xe^* and populate the upper laser level:

$$Xe_2^+ + e \rightarrow Xe(5d) + Xe, \qquad (5)$$

$$Xe\ Ar^+ + e \rightarrow Xe(5d) + Ar, \qquad (6)$$

which can be stimulated to emit a 1.73 μm photon corresponding on the $5d \rightarrow 6p$ transition

$$h\nu + Xe(5d[3/2]_1) \rightarrow Xe(6p[5/2]_2) + 2h\nu. \qquad (7)$$
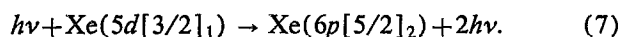
The upper levels and lower levels of the Ar-Xe laser transitions are 9–11 eV above the ground state of xenon, as shown in Fig. 1. At experimental conditions of 0.5% Xe and 860 Torr total gas pressure, the upper and lower levels have lifetimes of approximately 24 and 0.6 ns, respectively.[18] The dominant quenching process of the lower laser level is by collisional deexcitation by argon.[19]

To explain the observed high intrinsic efficiencies, several groups[1,8] have postulated electron recycling of the excited states in Xe. If the upper laser level were populated by direct electron impact from the ground state, the efficiencies would be lower than the 2%–6% measured. Electron recycling is viable in this system because Xe(6s) has a metastable lifetime of about 1 μs, which is long enough for it to act as a pseudoground state. Secondary electrons generated by the electron beam then ionize the long-lived Xe(6s). The Xe(6s) state is probably ionized by multiple

step electron impact ionization. For example, for a pump power of 100 W/cm^3 and assuming an average electron energy of 1 eV, the secondary electron density is of order 10^{13} cm^{-3}.[20] The cross section for exciting Xe(6s) by electrons is extremely large,[21] and the rate constant for electron impact excitation of Xe(6s) is about 10^{-6} cm^3/s, so this state will be excited up to a higher level in 10^{-7} s which is $\frac{1}{10}$ of the lifetime of this level. At 10 W/cm^3 the electron density is about three times smaller and the rate of exciting Xe(6s) up the ladder is three times longer. The measured increase in intrinsic efficiency from 2.2% at 85 W/cm^3 to 3.3% at 150 W/cm^3 may represent the onset of electron recycling.[5] Given the importance of the Xe(6s) level in the kinetics, a direct measurement of its population would be illuminating and should be feasible by resonant absorption.

However, if electron recycling and mixing of these states becomes very rapid, the excited states will come into a thermodynamic equilibrium with the secondary electrons.[2] It is for this reason that the efficiency initially increases as the pump power density increases from 10^2 to 10^3 W/cm^3 atm and then decreases at pump power densities greater than 10^4 W/cm^3 atm. This conclusion is consistent with the results of electron-beam-controlled discharge data of Perkins and Jacob[22] that show an increase in efficiency from 2% at 100 W/cm^3 to 6.3% at 700 W/cm^3 and the electron-beam data of Watterson and Jacob,[2] that show no lasing at pump power densities greater than 16 kW/cm^3 atm.

II. EXPERIMENTAL APPARATUS

A major objective of the experiment was to investigate the steady-state characteristics of an electron-beam-pumped, rare-gas laser and, thereby, the feasibility of long-pulse and cw operation at high output powers. An additional objective was to simulate the conditions of fission-fragment pumping. These goals required low pump power densities of 10–100 W/cm^3 and long-pulse durations of 0.1–1 ms. To achieve these operating parameters, an electron gun with a thermionic cathode was required.

A. Electron gun design

The electron gun in this experiment generated a current density of 0.2–5 mA/cm^2 in the laser gas mixture at a beam energy of 220 keV. The electron gun has four major components: a high-voltage capacitor, a high-voltage spark gap switch, a thermionic cathode, and a self-biasing grid for control of the electron-beam current. A schematic of the electron gun and the Ar-Xe laser cavity is shown in Fig. 2.

The high-voltage capacitor is a 240-m-long, high-voltage coaxial cable charged to −220 kV. For these experiments, the cable was simply employed as a 39 nF storage capacitor. The energy stored in the cable was delivered to the cathode structure through a trigatron spark gap switch pressurized with SF$_6$ and externally triggered. Rectangular high-voltage drive pulses were generated by minimizing circuit inductance and by utilizing a crowbar to terminate the electron beam at a preselected time.
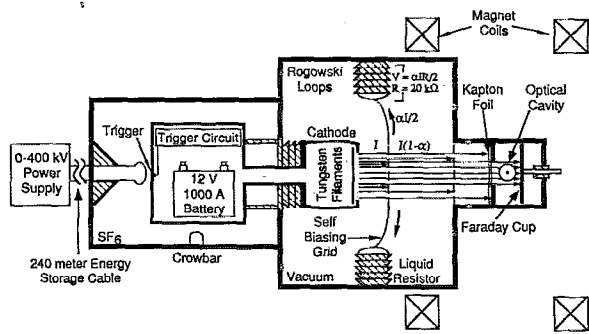
Thomas T. Perkins   4861

FIG. 2. Experimental layout showing the thermionic cathode used to produce a constant-current electron beam to pump an Ar-Xe laser.
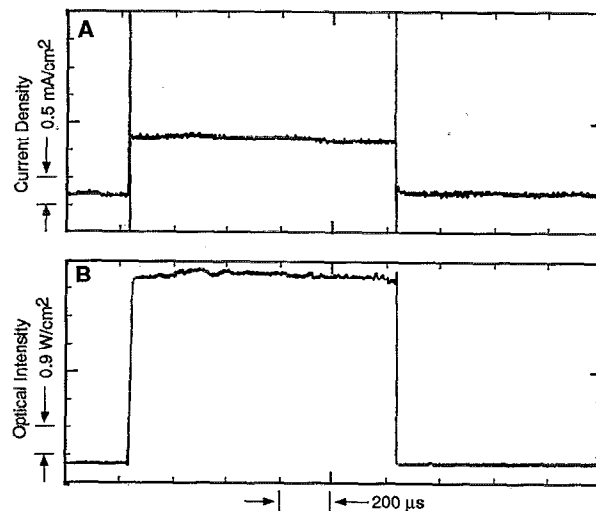

FIG. 3. A 1 ms, flat-top optical pulse demonstrates (a) the long-pulse, constant-current electron beam and shows (b) the resulting steady-state laser operation at 1.73 μm of 0.5% Xe at 860 Torr total cell pressure.

1. Thermionic cathode

The electron beam was generated from a thermionic cathode that consisted of an array of hot (2600 K), resistively heated tungsten filaments. With a thermionic cathode, a constant-impedance electron gun is achieved because, unlike cold cathodes that have a moving plasma front, the anode-cathode spacing is constant. The drawback to thermionic cathodes is simultaneously supplying the 10 kW needed to heat the filaments while they are charged to -220 kV. In this experiment, the filaments were heated by 1100 A supplied from lead acid battery. The battery, an automobile ignition coil in the trigatron spark gap circuit, and two optically controlled switches were enclosed inside the high voltage terminal. The metal enclosure acted as a Faraday cage, shielding the battery and trigger circuits inside. The high-voltage terminal was electrically connected through a vacuum feedthrough to the thermionic cathode. The cathode was fabricated from a linear array of 12-cm-long tungsten filaments with a 1.2 cm spacing. Although pure tungsten emits less current than thoriated tungsten at the same filament temperature, pure tungsten was found to be superior to thoriated tungsten for this application. Tungsten is less brittle, does not require an extended bakeout period, and is not easily poisoned.

2. Self-biasing grid

The electron gun operated in a triode configuration with a self-biasing grid that provided negative feedback to regulate the electron-beam current. The grid was located 10 cm from the cathode and controlled the emission of current from the thermionic cathode. The grid bias voltage was generated from the beam current intercepted by the grid and flowed to ground through two 20 kΩ liquid resistors connected in parallel. When the electron-beam current decreased, the current flowing through the bias resistors to ground also decreased. This resulted in a lower grid voltage and, thereby, an increased anode-cathode voltage. This increased anode-cathode voltage acted to restore the electron-beam current. By this method a constant-current electron beam was achieved. The effectiveness of this self-biasing triode configuration is demonstrated by the millisecond-long, electron-beam current pulses and the resulting flat-top optical pulses shown in Fig. 3. Pulse dura-

tion was limited only by the energy stored in the cable. The thermionic cathode appears to be a viable option for cw operation.

3. Power deposition diagnostics

The laser chamber was isolated from the high-vacuum, electron gun chamber by a 50-μm-thick Kapton foil. The electron beam entered the gas chamber through a 50×8 cm^2 opening and penetrated 6 cm through the gas where it was collected by a grounded aluminum plate in a manner analogous to a Faraday cup. The resulting current was measured by a Pearson current monitor as it returned to ground. The magnitude of the current was the same when measured in vacuum or at a pressure of 860 Torr. The aluminum plate was not flat, but serrated to suppress unwanted optical modes. The electron beam was confined by a 540 G magnetic field.

The power deposition in the gas was calculated by a Monte Carlo simulation,[23] using the experimental values of the current density and beam energy. To determine the beam energy, a capacitive voltage probe measured the cathode voltage and showed the expected exponential decay for a discharging capacitor. But, the pulses were terminated before the cathode voltage decreased by 10%. These Monte Carlo simulations showed the power deposition over the optical cavity was uniform to within 5%.

B. Optical cavity and laser output diagnostics

The optical cavity had a 50 cm gain length, a 70 cm mirror separation, and a 3.8 cm diameter. It consisted of a 10 m concave reflector ($R=99.8\%$ at 1.73 μm) and a flat partial reflector with a 1.73 μm antireflection coating on the rear surface. The mirrors were coated with narrow-band dielectric coatings on a BK7 or sapphire substrate. The cavity mirrors were used to seal the laser gas chamber, thereby avoiding the use of internal optical elements and

additional associated losses therein. Thus, the only losses were due to the nonsaturable absorption, the two cavity mirrors, and mirror misalignment. To minimize misalignment, a Davidson D275 autocollimator was used to align the laser cavity. A Molectron J50 pyroelectric energy meter was masked off to measure the central 0.635 or 0.953 cm of the optical beam 63 cm from the output of the optical cavity. A Judson J16 germanium detector operating at room temperature measured the optical pulse shape. An additional pyroelectric energy meter was placed directly behind the high reflectivity mirror to monitor for energy radiated at other wavelengths. The data was recorded on LeCroy 9400 digital oscilloscopes.

III. RESULTS AND DISCUSSION

The optics were optimized for 1.73 μm but there are other possible laser transitions. To ensure lasing occurred on only the 1.73 μm transition, the energy meter was placed directly behind the maximum reflector to measure energy at other wavelengths. The 99.8% reflector acted as a notch filter at 1.73 μm. This mirror transmitted 96% at 2.03 μm and an estimated 50% of the 2.65 μm line. No energy was measured by this meter. The optical energies measured at the output were thus due to the 1.73 μm radiation that is consistent with the measured gain-length product of 0.25–0.5. The losses were too large to achieve a net gain at wavelengths different from 1.73 μm. When broadband silver mirrors were used in the cavity, no optical energy at 1.73 μm was measured. Energy was measured only at 2.03 μm.[24]

A. Sensitivity to misalignment

At high reflectivities, small misalignments of less than 0.1 arcmin could reduce the laser intensity by 25%. This sensitivity is due to the low gain-length product ($g_0 L \approx 0.5$), the optical cavity configuration (10 m and flat), and the very high gain-to-loss ratio ($g_0/\alpha_{ns} > 1000$)—essentially no loss in the medium. We attribute the scatter in the data to such optical misalignment. The loss introduced by misalignment is dominant over $\alpha_{ns} \times L$ (≈ 0.001). If, after a preliminary analysis of the data, the intensities measured for a particular mirror were suspected of being low, additional data were taken on the realigned cavity. Only if four repeated shots were found to have a higher intensity would the original data be removed from the analysis.

B. Determination of g_0, Φ_{sat}, and α_{ns}

To calculate g_0, Φ_{sat}, and α_{ns}, the laser intensity was measured as a function of output mirror reflectivity for a given gas mixture and pump power density. Two to four shots were taken at each mirror reflectivity. The laser energy, optical pulse shape, and electron-beam current were recorded for each pulse. The output mirror reflectivity was varied from 31% to 98.6%. The dependence of g_0, Φ_{sat}, and α_{ns} on pump power density, Xe concentration, and total gas pressure was investigated. For consistency, all the pulses were 100 μs long. As shown in Fig. 4, such pulses
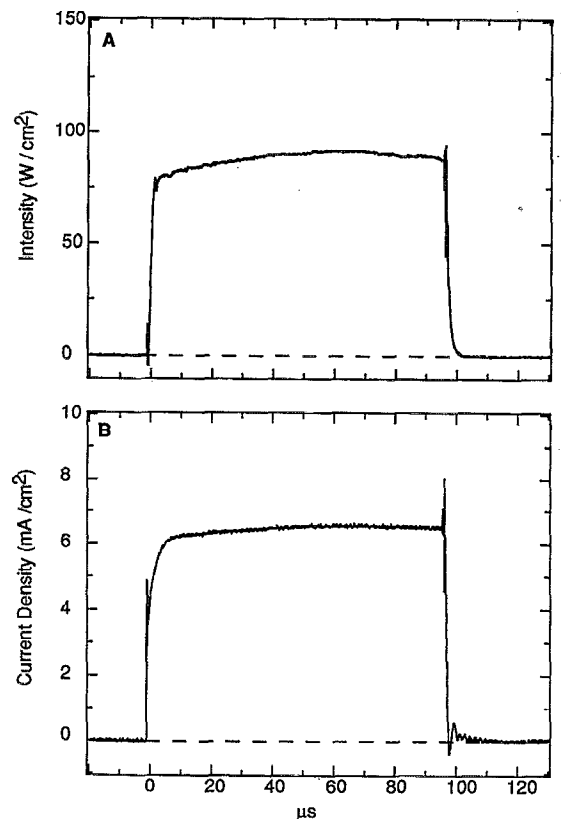

FIG. 4. A representative 100 μs pulse used in a Rigrod analysis showing (a) a steady-state optical intensity when (b) pumped by a constant-current electron beam for a gas mixture of 0.5% Xe in 860 Torr total gas pressure.

generated steady-state lasing over the entire pulse length. The maximum achieved efficiency—defined as the ratio of the measured optical energy extracted to the electron-beam energy deposited in the gas—was about 2.0% for the various laser mixtures and gas pressures investigated.

The g_0, Φ_{sat}, and α_{ns} were determined from the data by performing a three parameter, nonlinear fit[25] to the Rigrod formula

$$\Phi_{meas} = \Phi_{sat} \frac{(g_0 - \alpha_{ns})L + 0.5 \ln(R_1 R_2)}{1 - 2\alpha_{ns}L/\ln(R_1 R_2)}, \quad (8)$$

where Φ_{meas} is the measured intensity, L is the gain length (50 cm), R_1 is the reflectivity of the concave mirror, and R_2 is the reflectivity of the flat output coupler. The intensity measurements on each mirror were averaged, and each average Φ_{meas} was weighted equally in the analysis.[26] Representative fits are shown in Fig. 5 and results are summarized in Figs. 6 and Fig. 7.

The uncertainty for each variable was determined by an increase in χ^2 (see Refs. 27 and 28) and resulted in uncertainties of 4%–6% in small signal gain, 6%–10% in saturation flux, and 80%–200% in nonsaturable loss. The uncertainty in the loss was large because its absolute value was very small ($\alpha_{ns} \leqslant 0.001\%$/cm). Since the total loss was so small, losses due to scatter and absorption by the mirrors were expected to dominate. Rigrod's equation Eq. (8),
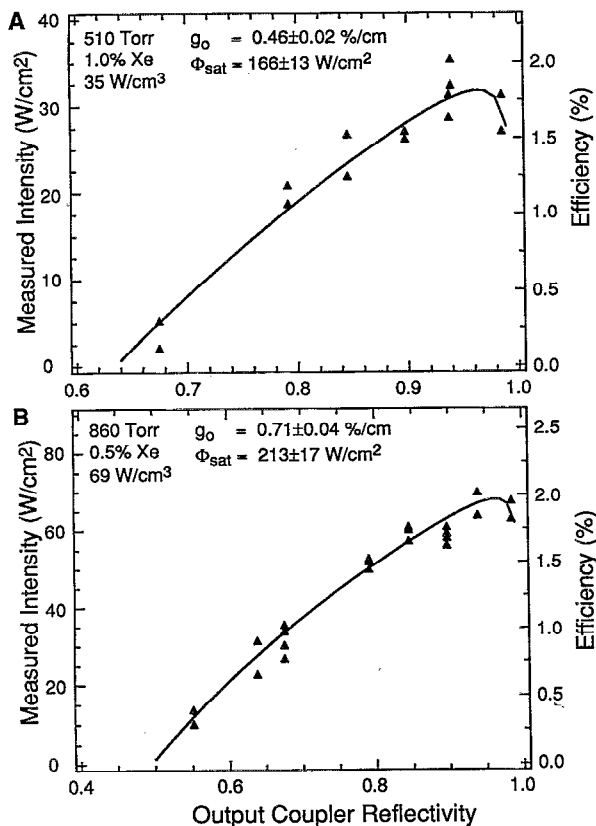
FIG. 5. Data and Rigrod fits to g_0, Φ_{sat}, and α_{ns} are shown for two different conditions: (a) 1.0% Xe in 510 Torr and (b) 0.5% Xe in 860 Torr total gas pressure. Both fits indicate an intrinsic efficiency ($g_0\Phi_{sat}/P$) of 2.2%, of which 90% was extracted, yielding measured efficiency of 2.0%. The nonsaturable absorption was zero to within experimental error.
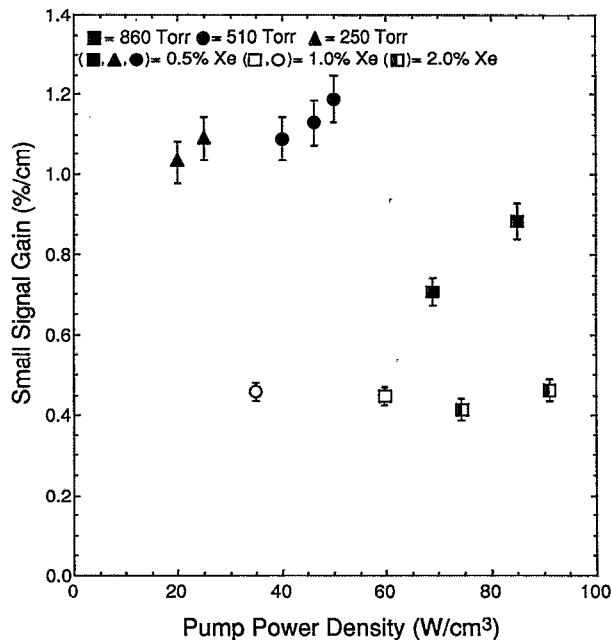

FIG. 6. Gain (g_0) as a function of pump power density. The measured gain varies inversely with both Xe concentration and with total cell pressure and varies proportionally to pump power density. The shape of the symbol indicates the total cell pressure. The shading determines the percentage of xenon.

$$g_0\Phi_{sat} = [\sigma\,(N_u - N_1)]\left[\left(\frac{h\nu}{\sigma\tau_u}\right)\right] = (h\nu)\,\frac{\Delta N}{\tau_u}, \qquad (9)$$

where σ is the stimulated emission cross section, N_u and N_l are the populations of the upper and lower laser levels,

was modified to allow for possible nondistributed loss. The effect of mirror losses from 0.0% to 0.4% per mirror were calculated. Losses per mirror of $\geqslant 0.2\%$ led to a negative value of α_{ns}. In summary, the calculated values of g_0 and Φ_{sat} changed by less than 1% as the loss per mirror was changed from 0.0% to 0.15%. A 1% variation in these calculated values is easily within the range of uncertainty for these variables. Thus, the results for g_0 and Φ_{sat} are insensitive to small mirror losses.

The dependence of the laser parameters on gas pressure could not be investigated at constant pump power densities. The power deposition in the laser gas is proportional to the total pressure. So, for the same electron-beam current, a reduction in the pressure led to a reduction in pump power density. Data were taken at total gas pressures of 250, 510, and 860 Torr.

C. Intrinsic efficiency and analysis of g_0 and Φ_{sat} results

To facilitate the comparison between each analysis, the intrinsic efficiency was computed by $\eta = g_0\,\Phi_{sat}/P$, where P is the pump power density and the product of $g_0\,\Phi_{sat}$ is just the stored optical power density:
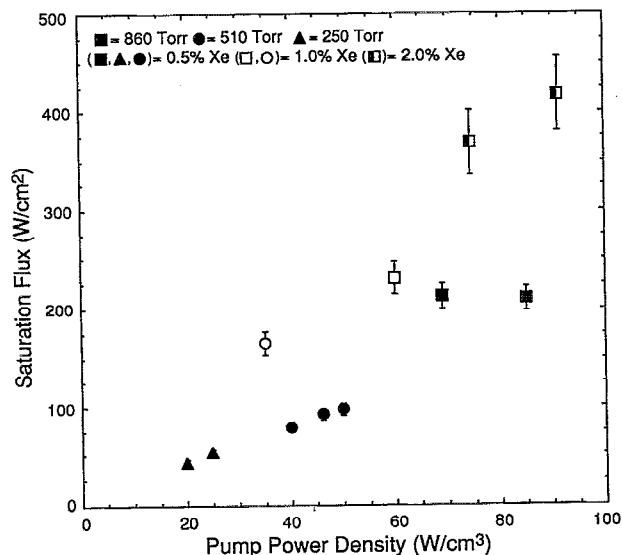

FIG. 7. Saturation flux (Φ_{sat}) as a function of pump power density. The measured saturation flux increases linearly with Xe partial pressure, as shown by the approximate doubling of Φ_{sat} the data between 0.5% and 1% Xe at ≈ 40 W/cm³ and the data between 1% and 2% Xe at ≈ 70–80 W/cm³. These results are consistent with Xe quenching dominating the lifetime of the upper laser level.
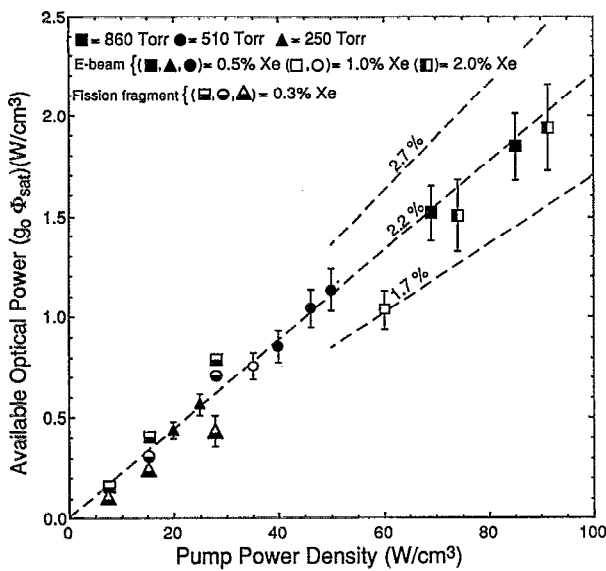
FIG. 8. Available optical energy ($g_0\Phi_{sat}$) as a function of pump power density. The intrinsic efficiency remains approximately constant at 2.2% over the full range of parameters investigated. The fission-fragment data are from Ref. 16, and the error bar is representative of the percentage error associated with the fission-fragment data. The total cell pressure for the fission-fragment data is approximate. The exact values are 260, 520, and 780 Torr.

respectively, and τ_u is the lifetime of the upper laser level. From this method, the intrinsic efficiency was computed to be 2.2% for 8 of the 11 experimental conditions, as shown in Fig. 8. Additionally for these flat-top pulses, power and energy efficiencies are equal.

It is useful to compare the maximum achieved efficiency and the intrinsic efficiency. The intrinsic efficiency refers to the stored optical energy per unit volume and, thus, the highest possible efficiency. The maximum achieved efficiency refers to the highest measured optical intensity divided by the product of the pump power density and the gain length. In this study, these two efficiencies differed by less than 10% because the gain-length product was much larger than the mirror and the alignment losses. The high circulating optical fluxes achieved at high output mirror reflectivities extracted the stored energy before the upper level was collisionally quenched or could spontaneously radiate. This is seen in Fig. 5, where the optical intensity peaks at very high reflectivity and shows, in part, why the optical intensity measurements were very sensitive to optical misalignments; at these high reflectivities, the losses introduced by the misalignment were significant in comparison to the losses due to the optical medium and the laser output coupler.

The principal experimental finding is that the intrinsic efficiency is essentially constant over the range of parameters explored. For instance, a decrease in g_0 was offset by an increase in Φ_{sat} as the gas mixture and pressure were changed. By understanding these changes, information on the dominant kinetics can be deduced. When the Xe concentration was doubled from 0.5% to 1.0% at 510 Torr at approximately equal pump power densities, Φ_{sat} approxi-

mately doubled from 76 W/cm^2 to 159 W/cm^2. Since Φ_{sat} increased by a factor of 2, τ_u must have been reduced by the same factor, verifying the sensitivity of τ_u to Xe partial pressure. The decrease in τ_u led to a reduction in the population inversion (ΔN) and, consequently, a reduction in g_0 from 1.75%/cm to 1.09%/cm. Further doubling the Xe concentration from 1% to 2% at 860 Torr led to a continued increase in Φ_{sat}, as seen in Fig. 7. Apparently, the effective lifetime of the upper laser level (τ_u) is dominated by Xe collisional quenching at these conditions. Intuitively, one expects Φ_{sat} to be proportional to the product of the linewidth times the decay rate from the upper laser level ($\Phi_{sat} \propto \Delta\nu\Gamma_u$). Experimentally, Hebner and Hays have shown the linewidth to be dominated by argon pressure broadening at these pressures.[29] Thus, in a simple model, Φ_{sat} should be proportional to the product of the pressure times the dominant quenching term. The results presented here are not consistent with both the quenching and the linewidth broadening being proportional to the argon pressure as shown by the sensitivity in Φ_{sat} to Xe concentration. From this data one can estimate that the rate constant for Xe quenching of the upper level by Xe is $\approx 10^{-10}$ cm^3/s. Clearly, a more complete explanation is necessary to describe these results and the data showing Φ_{sat} to increase linearly with pump power density.[16,30] Detailed kinetic models have been developed to more adequately describe the dependence of g_0 and Φ_{sat} on Xe partial pressure, total pressure, gas temperature, and pump power density.[31]

As shown in Fig. 6, the small signal gain increased when the pressure was reduced from 860 Torr (0.88%/cm) to 250 Torr (1.09%/cm) with the highest gain measured at 510 Torr (1.19%/cm). The gain increased in spite of the decrease in the electron-beam power deposition in the laser mixture caused by a reduction in gas pressure. At these pump rates, g_0 would be expected to be proportional to the pump power density which is proportional to the product of the electron-beam current times the total pressure. In part, this observed increase in g_0 can be understood as a reduction of the linewidth caused by collisional broadening as the total gas pressure is reduced from 860 to 250 Torr. Further, as discussed earlier, Xe quenching of the upper state reduced g_0 when the partial pressure of Xe was increased. For the same Xe concentration but lower total pressure, g_0 increases due to a lower Xe partial pressure. These results are in good agreement with gain measurements of Hebner and Hays which measured a 70% reduction in gain when the Xe concentration was increased from 0.3% to 3.0%.[16] The small signal gain continues to increase with decreasing Xe partial pressure until approximately 0.5–1 Torr of Xe at which point energy stored in the argon is not efficiently transferred to Xe.[9] Hebner and Hays have measured a 20%–40% reduction in gain when the Xe partial pressure was lowered from 1.5 to 0.15 Torr. In general, the measured gain varies inversely with both Xe partial pressure and with total cell pressure and varies proportionally to pump power density. However, this scaling of g_0 is limited to the experimental conditions is this study and does not fully describe g_0 measurements at pump power densities greater than 150 W/cm^3 where electron

Thomas T. Perkins   4865

mixing becomes important as demonstrated by an increase in intrinsic efficiency to 3.3%.[5,30]

D. Comparison to fission-fragment pumping

As stated earlier, one of the objectives of these long-pulse, low-power experiments is to simulate fission-fragment pumping. These electron-beam-pumped results will thus be compared with the most recent fission-fragment results of Hebner and Hays.[12,16] The fission-fragment measurements were taken at 260, 520, and 780 Torr gas pressure and an Xe concentration of 0.3%. However, the fission-fragment pump power density was lower (8–28 W/cm^3) than in these electron-beam experiments. As shown in Fig. 8, the fission-fragment results of Hebner and Hays and our electron-beam results show close agreement in intrinsic efficiency, except at 260 Torr. In general, the fission-fragment results showed a similar dependence of gain on Xe concentration and total cell pressure but, in general, a higher gain. When scaled for the differences in pump power density, the saturation fluxes for fission-fragment pumping were lower by approximately 50% than for electron-beam pumping at 520 Torr. For the most part, this difference is explained by Xe quenching that results from the higher Xe concentration used in our results (0.5% Xe) than in Hebner's results (0.3% Xe). The nominally close agreement between the results of fission-fragment and electron-beam pumping laser results validates the theoretically anticipated similarity in kinetics between these two different pumping methods.

IV. CONCLUSIONS

Steady-state lasing for 2.5 ms has been achieved in an electron-beam-pumped Ar-Xe laser. The results suggest that efficient, cw operation would be possible at low pump powers provided that the waste heat is removed by flowing gas. Steady-state values of g_0, Φ_{sat}, and α_{ns} were determined by a Rigrod analysis at different Xe concentrations, total gas pressures, and pump power densities. The results of g_0, Φ_{sat}, and α_{ns} presented in this article are generally consistent with previous research on a 1.73 μm Ar-Xe laser and provide detailed, steady-state measurements at low pump powers. The small signal gain varied inversely with both Xe partial pressure and with total cell pressure and varied proportionally to the pump power density. The saturation flux varied proportionally to the Xe partial pressure and total cell pressure. The intrinsic efficiency stayed approximately constant at 2.2% from 20 W/cm^3 to 85 W/cm^3. These results are consistent with Xe quenching of the upper laser level being the dominant deexcitation process. Further studies are planned to isolate the effects of total gas pressure and Xe partial pressure and to gain greater insight into these complicated laser kinetics.

ACKNOWLEDGMENTS

[1] N. G. Basov, V. A. Danilychev, A. Yu. Dudin, D. A. Zayarnyi, N. N. Ustinovskii, I. V. Kholin, and A. Yu. Chugunov, Sov. J. Quantum Electron. **14**, 1158 (1984).

[2] R. L. Watterson and J. H. Jacob, IEEE J. Quantum Electron. QE-26, 417 (1990).

[3] V. I. Derzhiev, A. G. Zhidkov, O. V. Sereda, V. S. Skakun, V. F. Tarasenko, A. V. Fedenev, and S. I. Yakovlenko, Sov. J. Quantum Electron. **20**, 902 (1990).

[4] E. L. Patterson, G. E. Samlin, P. J. Brannon, and M. J. Hurst, IEEE J. Quantum Electron. QE-26, 1661 (1990).

[5] T. T. Perkins, X. Chen, and J. H. Jacob, Conference on Laser and Electo-optics, Baltimore, MD, May 1991.

[6] L. N. Litzenberger, D. W. Trainor, and M. W. McGeoch, IEEE J. Quantum Electron. QE-26, 1668 (1990).

[7] N. N. Koval', Yu. E. Kreindel', G. A. Mesyats, V. S. Skakun, V. F. Tatasenko, V. S. Tolkachev, A. V. Fedenev, A. A. Chagin, and P. M. Shchanin, Sov. Tech. Phys. Lett. **12**, 16 (1986).

[8] S. A. Lawton, J. B. Richards, L. A. Newman, L. Specht, and T. A. DeTemple, J. Appl. Phys. **50**, 3888 (1979).

[9] T. T. Perkins and J. H. Jacob, 44th Gaseous Electronics Conference, Albuquerque, NM, Oct. 1991.

[10] J. E. Tucker and B. L. Wexler, IEEE J. Quantum Electron. QE-26, 1647 (1990).

[11] W. J. Alford and G. N. Hays, J. Appl. Phys. **65**, 3760 (1989).

[12] A. M. Voinov, L. E. Doubysh, V. M. Krivonosov, S. P. Melinokov, I. V. Podmoshenskii, and A. A. Sinyanskii, Sov. Tech. Phys. Lett. **7**, 437 (1981).

[13] G. A. Hebner and G. N. Hays, Conference on Lasers and Electro-Optics, Baltimore, MD, May 1991.

[14] T. J. Moratz and M. J. Kushner, J. Appl. Phys. **63**, 1796 (1988).

[15] M. Ohma, T. J. Moratz, and M. J. Kushner, J. Appl. Phys. **66**, 5131 (1989).

[16] G. A. Hebner and G. N. Hays, J. Appl. Phys. **73**, 3614 (1993).

[17] W. W. Rigrod, IEEE J. Quantum Electron. QE-14, 377 (1978).

[18] M. J. Kushner (private communication, 1990).

[19] W. J. Alford, J. Chem. Phys. **96**, 4330 (1992).

[20] Z. Rozenberg, M. Lando, and M. Rokni, Phys. Rev. A **35**, 4151 (1987).

[21] H. A. Hyman, Phys. Rev. A **18**, 441 (1978).

[22] T. T. Perkins and J. H. Jacob, Conference on Laser and Electo-optics, Anaheim, CA, May 1992.

[23] E. Salesky (private communication, 1990).

[24] E. L. Paterson and R. L. Watterson (private communication, 1991).

[25] W. H. Press, B. P. Flannery, S. A. Teokolsky, and W. T. Vetterling, *Numerical Recipes in C* (Cambridge University Press, Cambridge, 1988), Chap. 10.

[26] For the 2% Xe data, the measured intensity was a linear function of pump power density and the results were fit to a line. The value at a specific pump power density was determined from that line instead of averaging measurements within 5% of a specific pump power density.

[27] P. R. Bevington, *Data Reduction and Error Analysis for the Physical Sciences* (McGraw-Hill, New York, 1969).

[28] H. Cramer, *The Elements of Probability Theory* (Wiley, New York, 1955).

[29] G. A. Hays and G. N. Hays, Appl. Phys. Lett. **59**, 537 (1991).

[30] S. F. Fulghum, R. L. Watterson, T. T. Perkins, and J. H. Jacob, 45th Gaseous Electronics Conference, Boston, MA, Oct. 1992.

[31] J. W. Shon, M. J. Kushner, G. A. Hebner, and G. N. Hays, J. Appl. Phys. **73**, 2686 (1993).